High Activity and Wide Temperature Window of Fe-Cu-SSZ-13 in the Selective Catalytic Reduction of NO with Ammonia

Tao Zhang, Jianmei Li, Jian Liu, Daxi Wang, Zhen Zhao, and Kai Cheng
State Key Laboratory of Heavy Oil Processing, China University of Petroleum, Beijing 102249, China

Junhua Li
State Key Joint Laboratory of Environment Simulation and Pollution Control, School of Environment, Tsinghua University, Beijing 100084, China

DOI 10.1002/aic.14923
Published online July 14, 2015 in Wiley Online Library (wileyonlinelibrary.com)

Fe-Cu-SSZ-13 catalysts were prepared by aqueous solution ion-exchange method based on the one-pot synthesized Cu-SSZ-13. The catalysts were applied to the selective catalytic reduction (SCR) of NO with NH_3 and characterized by the means of XRD, UV-Vis, EPR, XPS, NH_3-TPD, and so on. The selected Fe-Cu-SSZ-13-1 catalyst exhibited the high NO conversion (>90%) in the wide temperature range (225–625°C), which also showed good N_2 selectivity and excellent hydrothermal stability. The results of XPS showed that the Cu and Fe species were in the internal and outer parts of the SSZ-13 crystals, respectively. The results of UV-Vis and EPR indicated that the monomeric Cu^{2+} ions coordinated to three oxygen atoms on the six-ring sites and Fe monomers are the real active species in the NH_3-SCR reaction. Furthermore, the influence of intracrystalline mass-transfer limitations on the Fe-Cu-SSZ-13 catalysts is related to the location of active species in the SSZ-13 crystals. © 2015 American Institute of Chemical Engineers *AIChE J*, 61: 3825–3837, 2015

Keywords: NH_3-SCR, NO conversion, Fe-Cu-SSZ-13, Fe monomers, reaction kinetics

Introduction

Nitrogen oxides (NO_x), which are emitted from the automobile exhaust gas and industrial combustion of fossil fuels, are harmful to the ecosystem and humans. The selective catalytic reduction (SCR) with NH_3 is an effective technique for the NO_x abatement from diesel exhaust or coal-fired power plants. V_2O_5-WO_3/TiO_2-based SCR catalysts have been commercially used for stationary source applications since 1970s.[1] However, there are still some inevitable problems existing in the V-based catalyst, such as the narrow working temperature window and the toxicity of vanadium species. Therefore, it is important to develop vanadium-free SCR catalysts for the removal of NO_x. Transition metal zeolite-based catalysts have been developed for mobile source applications because of their thermal stability and high NO_x reduction activity in a wide temperature range. In particular, copper-based zeolite catalysts have been found to be highly active at relatively low temperatures (<350°C). Moreover, iron-based zeolite catalysts have also been considered to be efficient SCR catalysts at high temperatures (>300°C). Unfortunately, these materials present low hydrothermal stability when reacting under harsh conditions (in the presence of steam at high temperatures).

In recent years, small pore zeolite-based Cu catalysts have become the hot subject of considerable study for commercial application of SCR catalysts.[2] Compared to aforementioned materials, they have been found to be more active and selective, and less prone to deactivation by hydrocarbon inhibition or thermal degradation.[3–6] For instance, Cu ion-exchanged SSZ-13 (Cu-SSZ-13), a zeolite with the Chabazite (CHA) structure containing small radius (~3.8 Å) eight-membered ring pores,[7] showed high activity in NO_x reduction activity. Conventionally, in Cu-SSZ-13 catalyst, the practical loading amounts of Cu play an important role in NH_3-SCR reaction. However, high Cu loading amounts in SSZ-13 zeolite is not easy, due to the small pore openings and limitation of ion-exchanged capacity. Recently, Xiao et al., He et al., and Corma et al. have nicely reported the direct preparation of Cu-SSZ-13 zeolite using a low-cost copper-amine complex (Cu^{2+} with tetraethylenepentamine, Cu-TEPA) as an efficient template.[8–14] This methodology allowed the direct introduction of extra-framework copper species in the CHA cages, thereby made the products with high copper content and good dispersion of copper species. This provides us a new and facile method to directly synthesize Cu-SSZ-13 zeolite with high Cu content for obtaining highly efficient SCR catalysts. However, the NO conversion over Cu-SSZ-13 catalyst decreases apparently above 450°C, probably due to the high oxidation activity of Cu species resulting in the NH_3 oxidation by oxygen. Thus, Cu-SSZ-13 catalyst should be further improved to remove NO_x which are emitted from the diesel engine in the process involving a sudden increase of the diesel exhaust

Jianmei Li has equal contribution as the first author.
Additional Supporting Information may be found in the online version of this article.

Correspondence concerning this article should be addressed to J. Liu at liujian@cup.edu.cn or Z. Zhao at zhenzhao@cup.edu.cn.

temperature above 500°C.[15] To further enhance the high-temperature activity of catalysts, it is necessary to introduce a second metal to Cu-SSZ-13 catalyst as an additive. Iron is one of the most interesting metals for enhancing the SCR catalytic activities at high temperatures. Sultana et al. confirmed that Fe-promoted Cu/ZSM-5 catalysts possessed high catalytic activity for high-temperature SCR of NO by NH_3.[16] Yang et al. found that for NH_3-SCR over Fe-Cu heterobimetallic zeolites, the excellent activity induced by iron addition could be correlated with the heteroatom in the vicinity of Cu^{2+}.[17] Zhang et al. prepared a series of Fe_x/Cu-SSZ-13 catalysts, which showed excellent deNO_x performance compared with Cu-SSZ-13.[18] Furthermore, the synergistic effect between Fe and Cu species was suggested. In our previous study, Fe was also found to improve the NO conversion at high temperatures for Fe_x-Cu_4/ZSM-5 catalysts.[19] Therefore, Fe-Cu-SSZ-13 catalysts may be a good candidate to achieve high NO conversion and N_2 selectivity in a wide temperature range.

Herein, Fe-Cu-SSZ-13 catalysts were prepared by aqueous solution ion-exchange method based on the one-pot synthesized Cu-SSZ-13 catalyst. The purpose of Fe addition to Cu-SSZ-13 is to further enhance the high-temperature activity of Cu-SSZ-13 catalyst. The locations of Cu and Fe species in Fe-Cu-SSZ-13 catalysts are investigated and the effects of different copper and iron species on the activity of NH_3-SCR are also evaluated. Furthermore, the low-temperature NH_3-SCR kinetics is studied on these catalysts under high-space velocity conditions. This kind of binary metal Fe-Cu-SSZ-13 is a promising catalyst for practical application in diesel engine emission control.

Experimental

Catalyst preparation

Cu-SSZ-13 catalyst was synthesized via one-pot synthesis.[8] Tetraethylenepentamine (TEPA) and $CuSO_4{\cdot}5H_2O$ were used to form a Cu-TEPA complex as a structure-directing agent. First, 0.771 g of $NaAlO_2$ and 0.50 g NaOH were added to dissolve into 7.945 g deionized water. The resulting solution was stirred at room temperature for 30 min. Then, 1.653 g $CuSO_4{\cdot}5H_2O$ and 1.505 g TEPA were added to the solution and stirred for 30 min. Next, 6.442 g of silica sol was added to the solution and stirred for 3 h. The resulting solution was transferred into Teflon-lined autoclaves and heated at a temperature of 140°C for 96 h. The product was recovered by vacuum filtration, washed with deionized water and dried at 100°C for 12 h. Then, the as-prepared precursor was dealt with different methods, which were described below.

The as-prepared precursor was directly calcined in air at 550°C for 8 h, labeled as Cu-SSZ-13. Fe-Cu-SSZ-13 catalysts were prepared by ion-exchange of Fe into Cu-SSZ-13. First, Cu-SSZ-13 was treated in a 1 mol/L solution of NH_4NO_3 to obtain NH_4^+/Cu-SSZ-13, labeled as Cu-SSZ-13-1 (The purpose of the preparation of Cu-SSZ-13-1 is to better show the effect of Fe addition on Cu-SSZ-13 catalyst. ICP analysis showed that copper weight percentage of Cu-SSZ-13-1 was 0.18%). Second, Fe ion exchange was performed by mixing Cu-SSZ-13-1 with a $Fe(NO_3)_3$ solution at ambient temperature for 8 h, and then were filtered and thoroughly washed with distilled water. The obtained samples were dried at 100°C for 12 h and calcined in air at 550°C for 6 h, and labeled as Fe-Cu-SSZ-13-1. Fe-Cu-SSZ-13-2 was prepared according to the same procedure, only different point was that Fe ion-exchange time was 12 h. In addition, the metal weight percentages in the catalysts were measured by ICP analyses.

To investigate the hydrothermal stability of the catalysts, the selected samples were heated from RT to 750°C at a ramp rate of 10°C/min and held for 16 h at 750°C in a flowing wet-air containing 10% H_2O.

Physical and chemical characterization

N_2 sorption isotherm was measured at 77 K using a Micromeritics ASAP 2020 instrument in static mode. The samples were degassed at 300°C for 8 h prior to the measurements. The specific surface area was calculated according to the Brunauer–Emmett–Teller (BET) method. The micropore volume was determined by the *t*-plot method (thickness range 0.34–0.40 nm).

Powder XRD patterns were obtained by a powder x-ray diffractometer (Shimadzu XRD 6000) using Cu Kα ($\lambda = 0.15406$ nm) radiation with a Nickel filter operating at 40 kV and 10 mA in the 2θ range of 5–40° at a scanning rate of 4°/min. The diffraction lines were identified by matching them with reference patterns in the JCPDS database.

UV-Raman spectra were recorded with a Renishaw Micro-Raman System 2000 spectrometer with spectral resolution of 2 cm^{-1}. The laser line at 325 nm of a He/Cd laser was used as exciting source with an output of 20 mW.

The measurements of Si/Al ratios were performed on an x-ray fluorescence (XRF) spectrometer MagiX (Philips).The actual content of Cu and Fe in catalysts were determined by inductive coupled plasma atomic emission spectrometry (ICP-AES; PE, OPTIMA 5300DV).

The surface morphologies of the catalysts were observed by field emission scanning electron microscopy on a Quanta 200F instruments using accelerating voltages of 5 kV. Samples for SEM were dusted on an adhesive conductive carbon belt attached to a copper disk and were coated with 10 nm Au prior to measurement.

The high resolution transmission electron microscopy (TEM) images were carried out using a JEOL JEM 2100 electron microscope equipped with a field emission source at an accelerating voltage of 200 kV.

Fourier transform infrared (FTIR) absorbance spectra were recorded in the wave numbers ranging from 4000 to 400 cm^{-1} via a FTS-3000 spectrophotometer manufactured by American Digilab company. The measured wafer was prepared as KBr pellet with the weight ratio of sample to KBr, 1/100. The resolution was set at 2 cm^{-1} during measurements.

The UV-Vis diffuse reflectance spectroscopy (UV-Vis DRS) experiments were performed on a UV-Vis spectrophotometer (Hitachi U-4100) with the integration sphere diffuse reflectance attachment.

X-ray photoelectron spectra (XPS) were recorded on a Perkin-Elmer PHI-1600 ESCA spectrometer using Mg Kα (hv = 1253.6 eV, 1 eV = 1.603×10^{-19} J) x-ray source. The binding energies were calibrated using C1s peak of contaminant carbon (BE = 284.6 eV) as an internal standard.

Nuclear magnetic resonance (NMR) spectra were recorded on a Bruker DMX-500 NMR spectrometer. For the ^{27}Al magic angle spinning (MAS) NMR a standard Bruker MAS probe head was used with rotor diameter of 2.5 mm, at a spinning rate of 20 kHz. The ^{27}Al chemical shift is referred to a saturated $Al(NO_3)_3$ solution. For ^{29}Si NMR measurement, the sample rotation rate was 10 kHz. Tetramethylsilane (TMS) was employed as an external reference for the chemical shift.

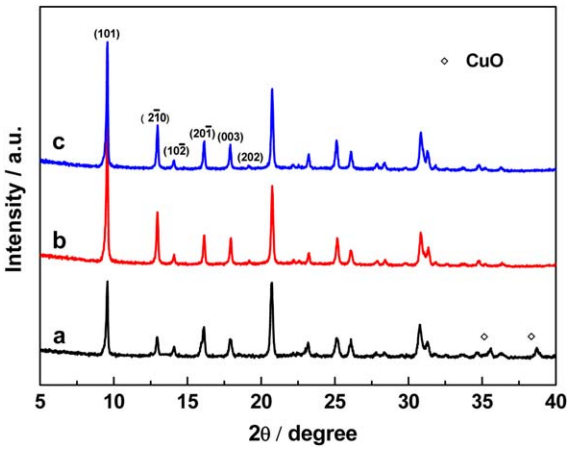

Figure 1. XRD patterns of Cu-SSZ-13 (a); Fe-Cu-SSZ-13-1 (b); Fe-Cu-SSZ-13-2 (c).

[Color figure can be viewed in the online issue, which is available at wileyonlinelibrary.com.]

Electron paramagnetic resonance (EPR) experiments were conducted on a Bruker X-band spectrometer equipped with a SHQE resonator and a continuous flow cryostat. Spectra were recorded at 123 K. Microwave power was 998 microwatts, and the frequency was 9.07 GHz.

The nature of the acid sites of the catalysts was determined by pyridine-IR on a MAGNAIR 560 FTIR instrument with a resolution of 1 cm^{-1}. The samples were dehydrated at 500°C for 5 h under a vacuum of 1.33×10^{-3} Pa, followed by adsorption of purified pyridine vapor at room temperature for 20 min. The system was then degassed and evacuated at different temperatures, and the Py-IR spectra were recorded.

Temperature-programmed reduction with H_2 (H_2-TPR) measurements were performed in a conventional flow apparatus. One hundred milligram sample was pretreated under air atmosphere by calcination at 300°C for 1 h and subsequently cooled to 30°C. Afterward, 10% H_2/Ar flow (40 mL/min) was passed over the catalyst bed while the temperature was ramped from 30 to 750°C at a heating rate of 10°C/min. The hydrogen consumption signal was monitored by a thermal conductivity detector (TCD). Before the outlet gases entering the TCD, a cooling trap and a filter packed with molecular sieve 5A (60–80 meshes) were used to remove H_2O and CO_2, respectively.

Temperature-programmed desorption of ammonia (NH_3-TPD) was performed in a conventional flow apparatus. Before TPD, each sample was pretreated with high-purity (99.999%) N_2 (40 mL/min) at 500°C for 1 h, then saturated with high-purity anhydrous ammonia at 100°C for 1 h and subsequently flushed with helium at the same temperature for 1 h to remove physisorbed ammonium. Finally, the TPD operation was carried out from 100 to 600°C at a heating rate of 10°C/min. The amount of NH_3 desorbed was monitored by a TCD.

Activity measurements

The NH_3-SCR activity measurements were carried out in a fixed bed quartz microreactor operating in a steady flow mode. The catalysts were sieved with 40–60 mesh and used in each test. The reactant gas composition included: 1000 ppm NO, 1000 ppm NH_3, 3% O_2, 5% H_2O (when used), and balance with N_2. The total flow rate was 500 mL/min and thus a normal gaseous hourly space velocity (GHSV) of 50,000 h^{-1} was obtained (0.4 g catalysts were used for evaluation), unless in the other cases to investigate the effects of H_2O and space velocity. The temperature varied from 100 to 700°C. The data were recorded when the SCR reaction reached steady state after 10 min at each measuring temperature. The concentrations of NO_x ($NO_x = NO + NO_2$) in the inlet and outlet gas mixture were measured by a SIGNAL4000 VM NO_x analyzer. Meanwhile, the concentrations of NH_3, NO, NO_2, and N_2O were measured by a FTIR spectrometer (MKS, MultiGas 2030HS). The NO conversion was calculated based on the inlet and outlet gas concentrations at steady state, as shown in Eq. 1

$$\text{NO Conversion} = \frac{[\text{NO}]_{\text{inlet}} - [\text{NO}]_{\text{outlet}}}{[\text{NO}]_{\text{inlet}}} \times 100\% \quad (1)$$

The N_2 selectivity in SCR reaction was calculated from Eq. 2

$$N_2 \text{ Selectivity} = \left(1 - \frac{2[\text{N}_2\text{O}]_{\text{outlet}}}{[\text{NO}_x]_{\text{inlet}} + [\text{NH}_3]_{\text{inlet}} - [\text{NO}_x]_{\text{outlet}} - [\text{NH}_3]_{\text{outlet}}}\right) \times 100\% \quad (2)$$

Results

The results of XRD and UV-Raman

The XRD patterns of Cu-SSZ-13 and Fe-Cu-SSZ-13 catalysts are shown in Figure 1. All the samples exhibit the typical XRD patterns of zeolites with the CHA framework topology,[20] indicating that the crystalline structure of as-synthesized Cu-SSZ-13 and Fe-Cu-SSZ-13 are essentially unchanged after ion-exchange treatments. For Cu-SSZ-13 (Figure 1a), two diffraction peaks located at 35.5° and 38.9° (labeled by open diamond symbol), and the both peaks can be related to CuO (PDF# 48-1548) phase. It suggests that the partial copper species, that is, CuO nanoparticles, locate on the external surface of Cu-SSZ-13 sample. No diffraction peaks of copper and iron species are observed for Fe-Cu-SSZ-13 samples, suggesting that copper and iron species should be either well dispersed or exit as isolated ions at the exchange sites. Meanwhile, the intensities of principal diffraction peaks of these samples increase after consecutive ion exchange. It is possibly due to that no copper and iron compounds on the surface of SSZ-13 absorb x-ray radiation.[21] Alternatively, it may be due to

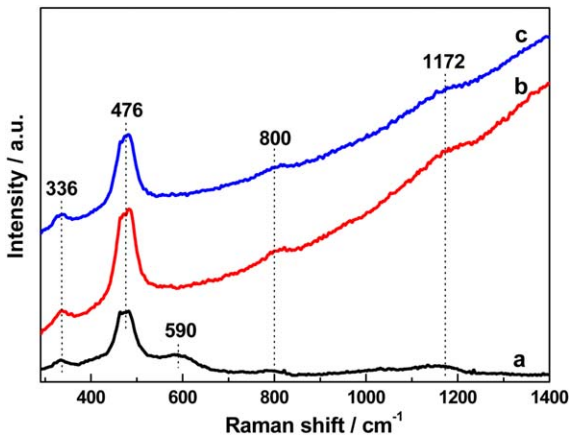

Figure 2. UV-Raman spectra of of Cu-SSZ-13 (a); Fe-Cu-SSZ-13-1 (b); Fe-Cu-SSZ-13-2 (c).

[Color figure can be viewed in the online issue, which is available at wileyonlinelibrary.com.]

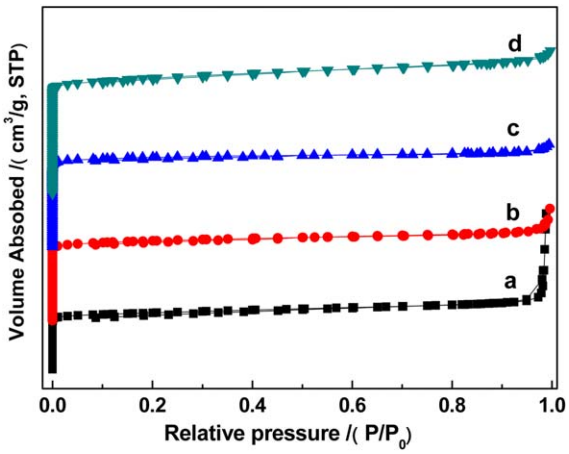

Figure 3. Nitrogen adsorption-desorption isotherms of Cu-SSZ-13 (a); Fe-Cu-SSZ-13-1 (b); Fe-Cu-SSZ-13-2 (c).

[Color figure can be viewed in the online issue, which is available at wileyonlinelibrary.com.]

recrystallization of the highly defective structures which generated during ion exchange.

Figure 2 shows the UV-Raman spectra of Cu-SSZ-13 and Fe-Cu-SSZ-13 samples. The spectra contain two intense bands at 336 and 476 cm^{-1} and two weak bands at 800 and 1172 cm^{-1}. The intense band centered at around 476 cm^{-1} is assigned to the v_s(T-O-T) mode (with T being Si or Al) of CHA zeolite. This band is typical for zeolite frameworks, consisting of a combination of four- or six- and eight-membered rings. The peak observed at 336 cm^{-1} is assigned to the T-O-T vibration mode of the six-membered rings of CHA zeolite. The weak and broad bands at 800 and 1172 cm^{-1} are typical symmetric and asymmetric Si-O vibration modes of zeolites, respectively. The spectrum of Cu-SSZ-13 contains an additional band at around 590 cm^{-1} (Figure 2a), which is the B_g mode of CuO nanostructures.[22] This is consistent with the XRD result that the Cu-SSZ-13 sample contains a small amount of CuO nanoparticles.

The results of BET

Figure 3 shows the adsorption-desorption isotherm curves of Cu-SSZ-13 and Fe-Cu-SSZ-13 samples. The textural properties derived from them are summarized in Table 1. All samples exhibit Type I isotherm corresponding to purely microporous materials, and the typical Langmuir-type adsorption indicates the presence of uniform micropores. Except for Cu-SSZ-13 with a BET surface area of 271.8 $m^3\ g^{-1}$, Fe-Cu-SSZ-13 samples have higher surface areas when treated with ion exchange, and the sample of Fe-Cu-SSZ-13-2 shows the highest BET surface area (545.7 $m^2\ g^{-1}$). Furthermore, the pore volume of Cu-SSZ-13, which was determined by the *t*-plot method, is 0.11 $cm^3\ g^{-1}$, whereas 0.22 $cm^3\ g^{-1}$ is available for Fe-Cu-SSZ-13-2 after ion exchange. The following reasons can account for these phenomena. Because the Cu loading in the initial Cu-SSZ-13 product resulting from one-pot synthesis was relatively high, some CuO nanoparticles formed on the surface of SSZ-13 in the untreated catalyst after direct calcination, which is proven by XRD and UV-Raman. Then, the formed CuO nanoparticles covered the external surface of SSZ-13 and clogged the micropores of SSZ-13 support. However, the results of XRD, UV-Raman, and ICP showed that most Cu species (especially CuO nanoparticles) were removed when Cu-SSZ-13 was treated by aqueous solution ion exchange, which results in the increase of the BET specific surface area and pore volume.

The results of SEM and HRTEM

Figure 4a shows the SEM images of Cu-SSZ-13 and Fe-Cu-SSZ-13 samples. Clearly, the different samples have similar morphologies, which consist of large cube-shaped crystals with sizes in the range of 1–3 μm. Most of the particles seem to be intergrown, which may be because the structures share a common plane of *d6r* rings. No visible damage is observed after ion exchange. The SEM images also confirm that the samples have been highly crystallized.

Figure 4b shows the HRTEM images of Cu-SSZ-13 and Fe-Cu-SSZ-13 samples. The spherical CuO nanoparticles anchored on the surface of Cu-SSZ-13 catalyst can be clearly observed in its HRTEM image, and partial CuO particles gather together with different sizes. The clear lattice fringe of CuO particle in HRTEM image was measured to be 2.31 Å indexed as (111) planes. Lattice fringes of CuO particle corresponding to (111) plane at 2.31 Å in fast Fourier transform (FFT) image indicates that supported CuO particles are crystallized and exposed (111) plane. After ammonium exchange and iron ion exchange, the copper and iron species are difficult to be distinguished on the surface of Fe-Cu-SSZ-13 samples (Figures 4b_2, b_3).

The results of MAS NMR

Solid-state NMR was used to monitor the differences in chemical environments of Al and Si in different SSZ-13 samples. The ^{27}Al MAS NMR spectra provide evidence for the framework connectivity of the aluminosilicate network. ^{27}Al MAS NMR spectra of Cu-SSZ-13 and Fe-Cu-SSZ-13 samples are shown in Figure 5a. The Al atoms are predominantly in tetrahedral coordination (Al^{IV}) as evidenced by the sharp resonance band at 57 ppm. The additional broad band around −1 ppm is related to extra-framework Al in octahedral coordination (Al^{VI}). Deconvolution of the ^{27}Al MAS NMR spectra shows that the 80% of the aluminum is at tetrahedral coordination in Cu-SSZ-13. Similar values (82% Al^{IV}) are obtained for

Table 1. Physicochemical Properties of Cu-SSZ-13, Cu-SSZ-13-1, and Fe-Cu-SSZ-13 Samples

Samples	($m^2\ g^{-1}$)[a]	V_{mic} ($cm^3\ g^{-1}$)[b]	SiO_2/Al_2O_3[c]	Cu (wt %)[d]	Fe (wt %)[d]
Cu-SSZ-13	271.8	0.11	7.40	8.27	–
Cu-SSZ-13-1	458.8	0.19	7.50	0.18	–
Fe-Cu-SSZ-13-1	497.5	0.21	7.46	0.14	0.089
Fe-Cu-SSZ-13-2	545.7	0.22	7.38	0.13	0.093

[a]Calculated by BET method.
[b]Calculated by *t*-plot method.
[c]Obtained from XRF technique.
[d]Obtain from ICP technique.

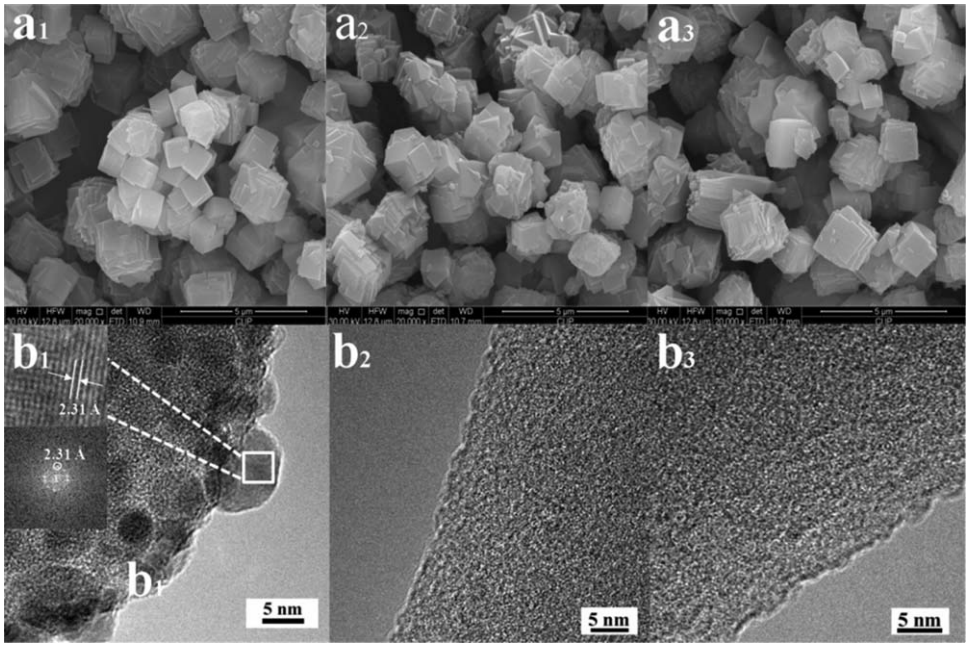

Figure 4. SEM images and HRTEM images of Cu-SSZ-13 (a_1, b_1); Fe-Cu-SSZ-13-1 (a_2, b_2); Fe-Cu-SSZ-13-2 (a_3, b_3).

The lattice fringes in an image correspond to (111) plane of CuO particle at 2.31 Å. The one in an image shows a CuO particle whose lattice fringes correspond to (111) plane at 2.31 Å in FFT image.

Fe-Cu-SSZ-13 samples, but a much larger fraction of Al is tetrahedral coordination (100%) for Cu-SSZ-13-1 sample (Supporting Information Figure S2), suggesting that no resonances of extra-framework octahedral Al^{3+} exist in this sample. The results indicate that extra-framework aluminum was removed during ammonium exchange. However, the dealumination of the framework took place during Fe ion exchange. Moreover, the appearance of octahedral Al^{3+} in Fe-Cu-SSZ-13 samples strongly suggests that paramagnetic irons may interact more strongly with framework aluminum than the formed octahedral Al^{3+}.

^{29}Si MAS NMR technique was used to gain further insight on the local environment of Si sites in the different samples. The results obtained on Cu-SSZ-13 and Fe-Cu-SSZ-13 samples are shown in Figure 5b. The NMR peak at −90.8 ppm comes from isolated Si, that is, the $Si(OAl)_4$ groupings (Q_0) in samples with stronger signals in the range from −95 to −110 ppm. These are assigned to $Si(OSi)(OAl)_3$ (−95.1 ppm, Q_1), $Si(OSi)_2(OAl)_2$ (−99.7ppm, Q_2), $Si(OSi)_3(OAl)$ (−104.8 ppm, Q_3), and $Si(OSi)_4$ (−109.5 ppm, Q_4) sites.[23] These features may demonstrate the existence of various Si species within these samples, whereas the existence of the $Si(OAl)_4$ species indicates that the obtained CHA-type samples have a high aluminum content. Furthermore, the growth of the peaks at chemical shifts of −109.5 ppm after ammonium exchange and Fe ion exchange, demonstrates some irreversible hydrolysis occurring during ion exchange. The results are fully consistent with the XRD, surface area, and pore volume measurements.

The results of UV-Vis DRS

UV-Vis DRS spectroscopy was applied to understand the nature and coordination of copper and iron species in the samples. Figure 6 shows the UV-Vis absorption spectra of Cu-SSZ-13 and Fe-Cu-SSZ-13 catalysts. They show two different bands: a broad band between 540 and 800 nm and a narrow one with the center at about 220 nm. The first absorption band is normally attributed to d-d transitions of Cu^{2+} ions in a

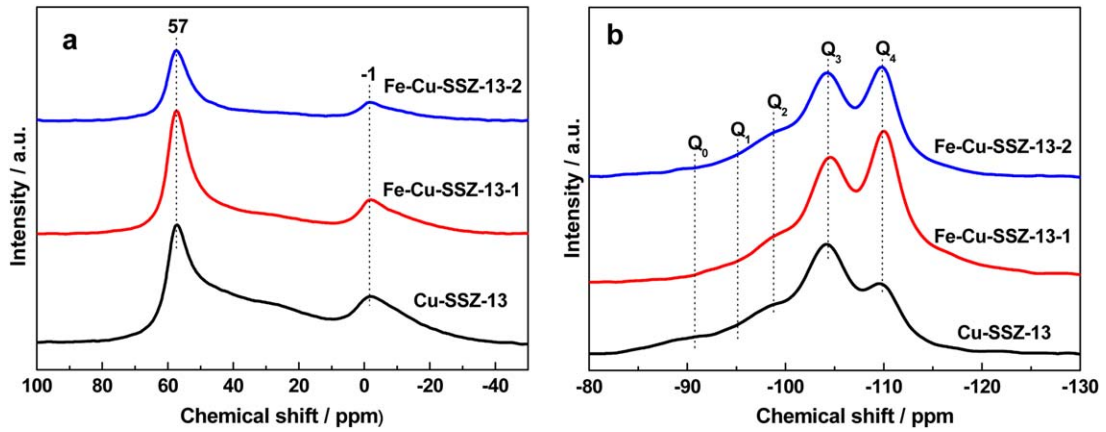

Figure 5. ^{27}Al MAS NMR spectra (a) and ^{29}Si MAS NMR spectra (b) of Cu-SSZ-13 and Fe-Cu-SSZ-13 samples.

[Color figure can be viewed in the online issue, which is available at wileyonlinelibrary.com.]

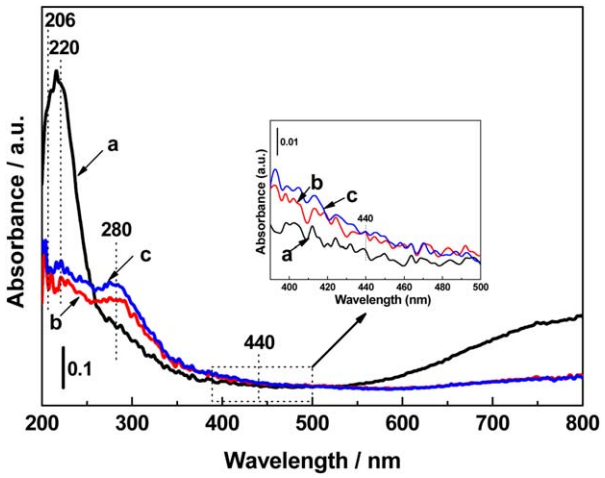

Figure 6. UV-Vis DRS spectra of Cu-SSZ-13 (a); Fe-Cu-SSZ-13-1 (b); Fe-Cu-SSZ-13-2 (c).

[Color figure can be viewed in the online issue, which is available at wileyonlinelibrary.com.]

pseudo-octahedral ligand oxygen environment, which is assigned to copper species in the extra-framework position (dispersed CuO particles).The second absorption band centered at about 220 nm is due to the charge transfer band related to O → Cu transition from lattice oxygen to isolated Cu^{2+} ions.[24]

In addition, Fe-Cu-SSZ-13 catalysts have two absorption bands that can be attributed to isolated tetrahedral and octahedral Fe^{3+}centered at about 206 and 280 nm, respectively, as seen in Fe-ZSM-5-type structures.[25] Signals between 300 and 400 nm have been assigned to small oligomeric clusters, which are not present in Fe-Cu-SSZ-13 catalysts. In general, absorption bands of iron oxide clusters are believed to be above 400 nm. They are also not observed, suggesting these iron species are scarcely present on the surface of Fe-Cu-SSZ-13 catalysts. This observation is in good agreement with the results of XRD and HRTEM.

The results of XPS

To explore the chemical environment of Cu and Fe elements on the surface of Cu-SSZ-13 and Fe-Cu-SSZ-13 catalysts, XPS spectra were measured. Figure 7 depicts the Cu 2p XPS spectra of the different samples. The Cu 2p spectrum of Cu-SSZ-13 sample shows the typical structure for copper species with broad main peaks (Cu $2p_{3/2}$ and Cu $2p_{1/2}$) and typical shake-up satellites. The Cu $2p_{3/2}$ signal is composed of two peaks at 933.0 and 935.8 eV. The former one is assigned to the presence of CuO species, and the latter one is attributed to Cu^{2+} ions coordinated to superficial oxygen atoms of the zeolite (Cu-O-Si-O).[26,27] The Cu $2p_{3/2}$ and Cu $2p_{1/2}$ peaks are accompanied by distinct shake-up satellites at about binding energy of 944 and 963 eV, which are the characteristic of Cu^{2+}. These characteristic satellites can be attributed to the charge transfer between the transition metal 3d and surrounding ligand oxygen 2p orbitals.[28] The results testified that a part of copper species were incorporated into the framework in the form of Cu-O-Si-O in Cu-SSZ-13 sample. Figures 7b, c confirm the absence of Cu species on the external surface of Fe-Cu-SSZ-13 catalysts.

The XPS spectra of Fe 2p of Fe-Cu-SSZ-13 catalysts are shown in Figures 7d, e. For Fe 2p XPS spectra, each peak (Fe $2p_{3/2}$ and Fe $2p_{1/2}$) can be decomposed into a doublet and one broad asymmetric shake-up satellite. One of the Fe $2p_{3/2}$ doublet peaks is at 710.8 eV and the second one is at 713.8 eV. These values are close to those of the binding energies of Fe $2p_{3/2}$ in FeO and Fe_2O_3, indicating that the iron ions in Fe-Cu-SSZ-13 are present in two valances of +2 and +3.[29] The results of XPS also suggest that the value of *R* (the Fe species ratio of Fe^{2+}/Fe^{3+}) decreases from 2.509 (Fe-Cu-SSZ-13-1) to 1.532 (Fe-Cu-SSZ-13-2) in Table 2. Nedyalkova et al. demonstrated that the low-temperature NO reduction was found to be closely related to the Fe^{2+}/Fe^{3+} ratio. Based on spectroscopic studies,[30] Rivallan et al. showed that NO interacts with isolated Fe^{2+} centers in formation of tri-nitrosylic and di-nitrosylic complexes,[31] while Fe^{3+} forms only a mono-nitrosylic complex. The difference in the capability of Fe^{2+} and Fe^{3+} to interact with NO and further react with stored ammonia might be also an important factor for NH_3-SCR activity at low temperatures.

The results of EPR

The hyperfine structure of isolated Cu^{2+} species can be characterized by EPR spectroscopy, while all the other copper species (e.g., copper oxide and Cu^{+} ions) will not exhibit any EPR signals. Therefore, EPR is an excellent technique to quantitatively identify the amount of isolated Cu^{2+} and to

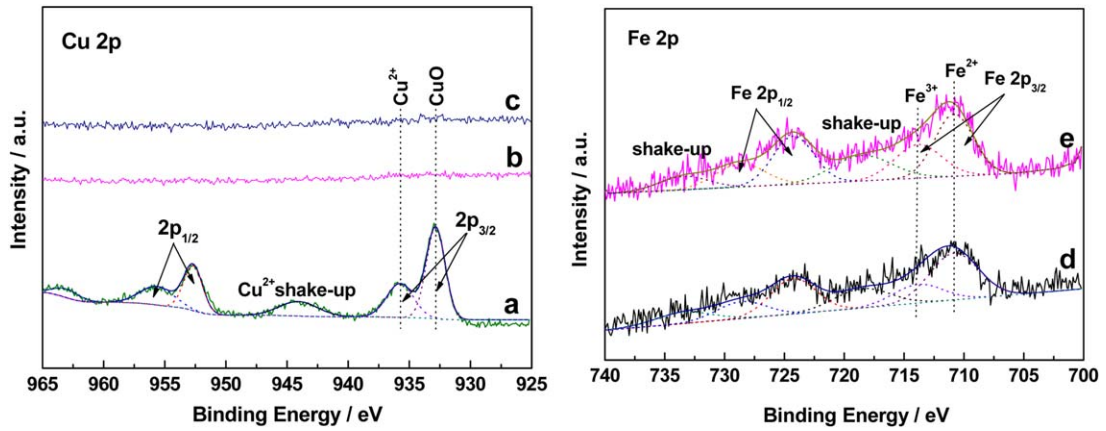

Figure 7. Cu 2p XPS spectra of Cu-SSZ-13 (a); Fe-Cu-SSZ-13-1 (b); Fe-Cu-SSZ-13-2 (c). Fe 2p XPS spectra of Fe-Cu-SSZ-13-1 (d); Fe-Cu-SSZ-13-2 (e).

[Color figure can be viewed in the online issue, which is available at wileyonlinelibrary.com.]

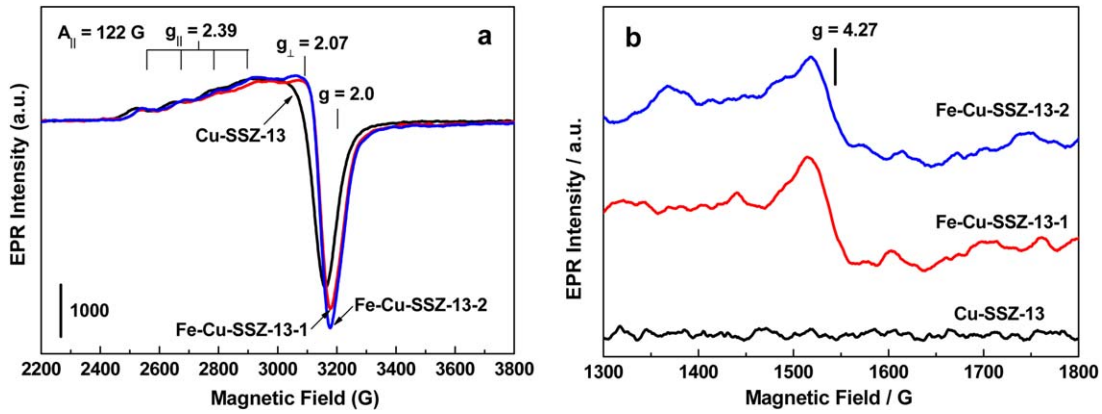

Figure 8. Cu^{2+} EPR spetra (a) and Fe^{3+} EPR spetra (b) of Cu-SSZ-13 and Fe-Cu-SSZ-13 samples measured at 123 K.

[Color figure can be viewed in the online issue, which is available at wileyonlinelibrary.com.]

probe the structure and coordination environment of paramagnetic isolated Cu^{2+} ions in Cu-zeolite catalysts.[32] As shown in the EPR spectra (Figure 8a), Cu^{2+} species in Cu-SSZ-13 catalyst show axial symmetry for all the spectra, four adsorption peaks in the parallel region and a sharp peak in the vertical region are observed. As the perpendicular components for the individual signals mostly overlap strongly, their parameters could not be exactly evaluated. According to the EPR spectra and literature reports,[33] the EPR signals at $g_{||} = 2.39$, $A_{||} = 122$ G and $g_{\perp} = 2.09$ on Cu-SSZ-13 catalyst could be ascribed to Cu^{2+} coordinated to three oxygen atoms on the six-ring sites. For Fe-Cu-SSZ-13 catalysts, the Cu^{2+} EPR spectra (Figure 8a) are similar to that of Cu-SSZ-13 catalyst with a signal at $g_{||} = 2.39$ and resolved fine-hyperfine coupling. However, the value of $g_{\perp}$ shifts to 2.07, due to the superimposed and broad signal at $g = 2.0$, which is the characteristic EPR signal for Fe species.

The Fe^{3+} EPR spectra of Fe-Cu-SSZ-13 catalysts are exhibited in Figure 8b. Compared with the signal in Cu-SSZ-13, the high EPR intensity of the signal at $g = 4.27$ of Fe-Cu-SSZ-13, generally observed in EPR of Fe-ZSM-5,[27] suggests tetrahedral Fe^{3+} exist in Fe-Cu-SSZ-13. Tuel et al. reported that the EPR signal at $g = 4.27$ corresponds to the strongly rhombic distorted tetrahedra $[FeO_4]^-$ and is originating from the lowest and the middle Kramers doublet.[34] In addition, the $g = 2.0$ signal (Figure 8a) is probably a superposition of two signals. The one has sharp signal from iron ions with only axially distorted octahedral or tetrahedral coordination geometry and the other one has broad signal from iron oxygen oligomers.[35] Nevertheless, the oligomers are paramagnetic at high temperatures and antiferromagnetic at low temperatures while the iron ions are purely paramagnetic. Thus, the signal from oligomers diminishes upon cooling to 123 K, while the signal from iron ions increases. Due to the Fe-Cu-SSZ-13 samples were measured at 123 K, it can be concluded that the $g = 2.0$ signal is from iron ions with only axially distorted octahedral or tetrahedral coordination geometry.

Table 2. Surface Composition and Oxidation State of Fe 2p Species Over Fe-Cu-SSZ-13 Catalysts from XPS Analyses

	Fe Species		
Sample	Fe^{2+}	Fe^{3+}	R^a
Fe-Cu-SSZ-13-1	71.5	28.5	2.509
Fe-Cu-SSZ-13-2	60.5	39.5	1.532

[a]Determined by the Fe species ratio of the Fe^{2+}/Fe^{3+}.

The results of NH_3-TPD

The acidity of the zeolites is one of the important parameters that determine the extent of NO_x reduction with ammonia over zeolite-based catalysts.[36] NH_3-TPD was carried out to determine the strength and amount of different acid sites. As shown in Figure 9, the NH_3-TPD curves of all the samples contain three desorption peaks. The peaks below 250°C can be assigned to weakly adsorbed NH_3 or ammonium species adsorbed at weak Lewis acid sites.[31] The peaks in the temperature range of 350–450°C could be attributed to ammonia adsorbed at strong Brønsted acid sites.[37,38] The peaks above 470°C might be due to strong Lewis acid sites originated from the high dispersion of copper and iron species or could account for especially strong Brønsted acid sites formed by the interaction of Brønsted acid sites with extra-framework aluminum species.[39–41] Supporting Information Figure S4 shows that the peaks (above 470°C) of Cu-SSZ-13-1 and Fe-Cu-SSZ-13 samples are similar with each other. However, the ^{27}Al NMR spectra of Cu-SSZ-13-1 (Supporting Information Figure S2) and Fe-Cu-SSZ-13 (Figure 5) revealed that almost all Al atoms were in the framework of Cu-SSZ-13-1 sample

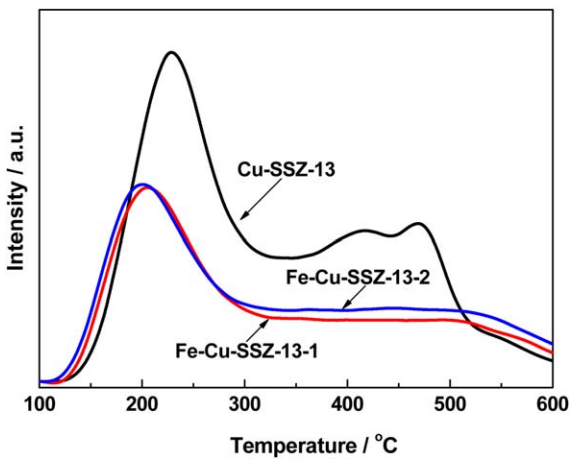

Figure 9. NH_3-TPD curves of Cu-SSZ-13 and Fe-Cu-SSZ-13 samples.

[Color figure can be viewed in the online issue, which is available at wileyonlinelibrary.com.]

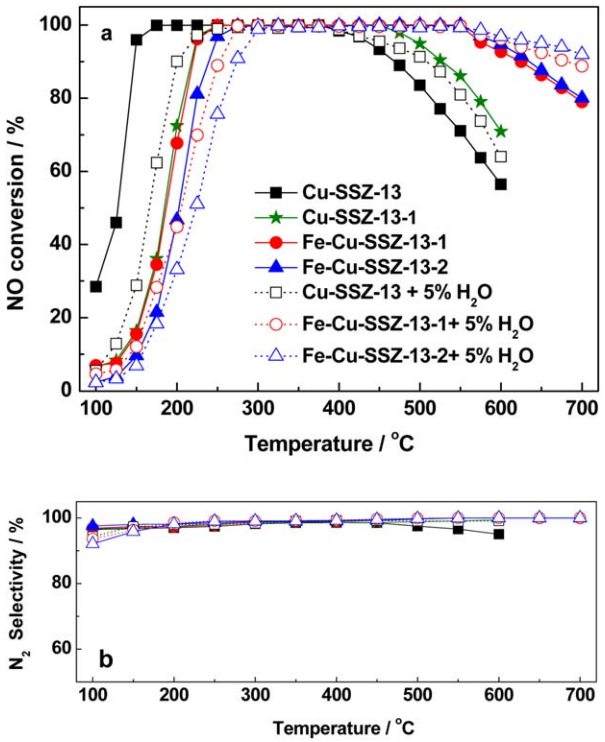

Figure 10. NO conversion (a) and N_2 selectivity (b) as a function of temperature over Cu-SSZ-13, Cu-SSZ-13-1, and Fe-Cu-SSZ-13 catalysts.

[Color figure can be viewed in the online issue, which is available at wileyonlinelibrary.com.]

whereas the Fe-Cu-SSZ-13 samples had some extra-framework aluminum. Thus, it can be concluded that the peaks above 470°C are attributed to the Lewis acid sites which are introduced by the high dispersion of copper and iron species.

The intensities of all peaks of Fe-Cu-SSZ-13 catalysts are much lower than that of Cu-SSZ-13. This indicates that ion-exchange treatments of Cu-SSZ-13 catalyst would first result in the change of the amount of active species, and then cause the change of catalyst acidity. At the same time, the peak above 470°C shifts to higher temperature, suggesting that the strength of Lewis acid sites on Fe-Cu-SSZ-13 is stronger and the copper and iron species in Fe-Cu-SSZ-13 are more stable.[9] The intensity of the NH_3 desorption peaks obtained for Fe-Cu-SSZ-13-2 catalyst is slightly stronger than those observed for Fe-Cu-SSZ-13-1 catalyst, which suggests that the NH_3 storage capacity (area under the curve) of Fe-Cu-SSZ-13-2 is relatively higher than that of Fe-Cu-SSZ-13-1.

NH_3-SCR catalytic activity

Figure 10a shows the NO conversion as a function of reaction temperature over Cu-SSZ-13 and Fe-Cu-SSZ-13 catalysts. The high NO conversion (>90%) over Cu-SSZ-13 is obtained in the temperature range of 150–450°C and then it decreases significantly with the increasing of temperature since the consumption of ammonia due to its oxidation.

Compared with Cu-SSZ-13, Fe-Cu-SSZ-13 catalysts show higher NO conversion at high temperatures, owing to iron species being introduced. Meanwhile, their NO conversion decreases distinctly at low temperatures, which may be due to a large number of active Cu species being exchanged. Moreover, the N_2 selectivities of Cu-SSZ-13 and Fe-Cu-SSZ-13 catalysts (Figure 10b) are above 90%. Thus, it is possible to control the temperature window range for NO conversion by controlling the content of Cu and Fe species. If NO conversion is desired at low temperatures, the presence of more copper species seems to be helpful, whereas at high temperatures the presence of more iron species is desired.

For the actual diesel engine exhaust system, the content of H_2O generated from the combustion of diesel fuel with a high carbon number is distinctive in the gas stream. Thus, the NH_3-SCR performances of Cu-SSZ-13 and Fe-Cu-SSZ-13 catalysts were tested in the presence of H_2O, as also shown in Figure 10a. The presence of 5% H_2O decreases the NO conversion significantly at low temperatures mainly due to the competitive adsorption by H_2O, and the NO conversion is increased at high temperatures probably due to the inhibition effect of H_2O on the unselective catalytic oxidation of NH_3.[42,43] Furthermore, the N_2 selectivities of Cu-SSZ-13 and Fe-Cu-SSZ-13 catalysts (Figure 10b) are also above 90% in the presence of H_2O. Figure 11 shows the SCR activities of Cu-SSZ-13 and Fe-Cu-SSZ-13-1 before and after hydrothermal aging. NO conversion of hydrothermally treated samples decreases in the whole temperature range. However, Fe-Cu-SSZ-13-1-aged still achieves more than 80% NO conversion from 250 to 525°C. By contrast, NO conversion of Cu-SSZ-13-aged decreases significantly and the maximum NO conversion is only 42.3% in the whole temperature range. This result can be related to Cu content and the addition of Fe.

Cu-SSZ-13 and Fe-Cu-SSZ-13 catalysts are good on both activity and selectivity for SCR of NO with ammonia. However, CHA catalysts have severe intracrystalline mass-transfer limitations due to the small-pore opening structure of CHA,[44,45] so the kinetics research of SCR reactions was first conducted to search for kinetically benign (i.e., mass-transfer limitation free) regimes. Figure 12a shows the standard SCR reaction results for Fe-Cu-SSZ-13-1 catalyst at various space velocities. In the absence of interparticle mass-transfer limitations, NO conversion is expected to increase by *n*-fold as the space velocity decreases by *n*-fold.[44] Based on this criterion, NO conversion ratios (Figure 12b) suggest that, for Fe-Cu-SSZ-13-1, interparticle mass-transfer limitation is more than

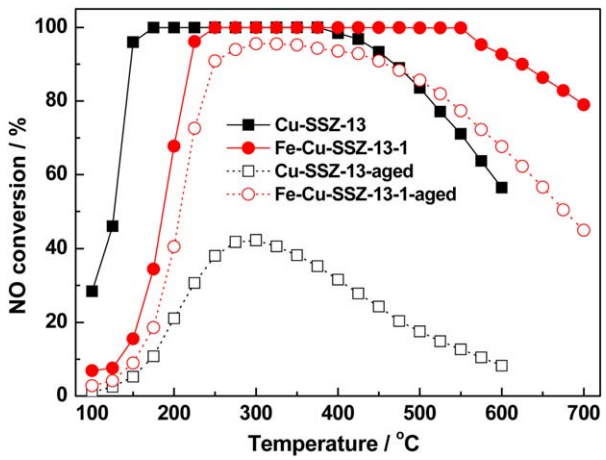

Figure 11. NO conversion as a function of temperature over Cu-SSZ-13 and Fe-Cu-SSZ-13-1 catalysts before and after hydrothermal aging at 750°C.

[Color figure can be viewed in the online issue, which is available at wileyonlinelibrary.com.]

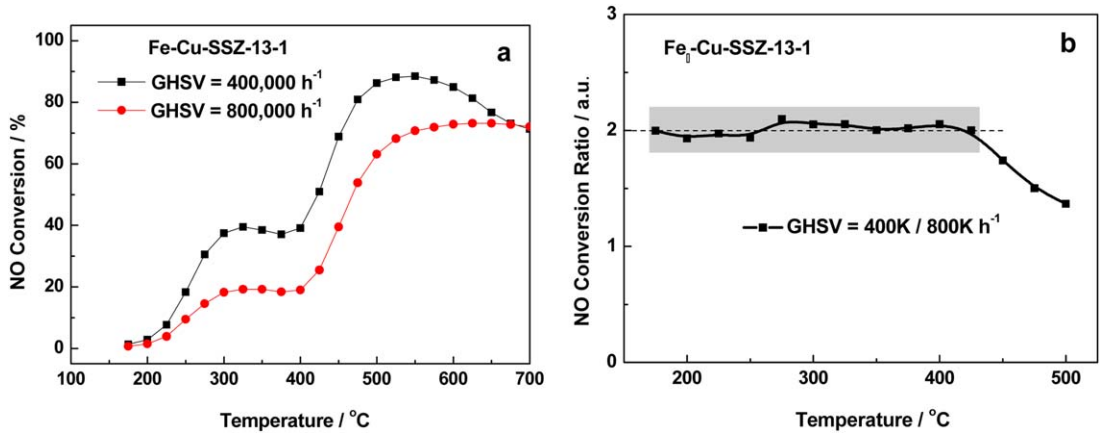

Figure 12. (a) NO conversion vs. reaction temperature for standard NH_3-SCR over Fe-Cu-SSZ-13-2 sample at space velocities of 400,000 and 800,000 h^{-1}; (b) NO conversion ratios for GHSV of 400,000 and 800,000 h^{-1} as a function of reaction temperature, using data from (a).

[Color figure can be viewed in the online issue, which is available at wileyonlinelibrary.com.]

95% free under the condition of GHSV $\geq$ 400,000 h^{-1} and temperature $\leq$ 425°C.

Figure 13 shows the reaction results of standard SCR at a high-space velocity (~800,000 h^{-1}) over Cu-SSZ-13 and Fe-Cu-SSZ-13 catalysts. NO conversion over Cu-SSZ-13 is much higher than that over Fe-Cu-SSZ-13 samples below 500°C. Meanwhile, NO conversion levels off at reaction temperatures above 300°C over Cu-SSZ-13 sample and decreases distinctly at 450°C and above. However, NO conversion levels off at reaction temperatures above 275°C over Fe-Cu-SSZ-13 samples and increases distinctly above 425°C. This difference is attributed to that the high copper content of Cu-SSZ-13 sample are favorable for SCR reaction in the low temperature range, but nonselective NH_3 combustion would happen in the high temperature range.[3,7]

Turnover frequency (TOF) was estimated by dividing the moles of NO molecules converted per second by the moles of Cu or Cu+Fe atoms in the catalysts. NO conversion over Cu or Cu+Fe sites in a catalyst is determined by ignoring the conversion over pure SSZ-13 from the total conversion over the catalyst. To calculate TOF values, the active sites should be identified and quantified. However, this is almost impossible even if active species are well dispersed, because all Cu or Cu+Fe atoms are not equally active. Therefore, we use the "apparent TOF" to assess an "average" efficiency of Cu or Cu+Fe in different catalysts for catalyzing the reaction. Arrhenius plots are depicted in Figure 14. Cu-SSZ-13, Fe-Cu-SSZ-13-1, and Fe-Cu-SSZ-13-2 catalysts give different apparent activation energies, suggesting that the reaction rate is related to Cu and Fe loading. Compared Cu-SSZ-13-1 (Supporting Information Figure S6) with Cu-SSZ-13, the increase in TOF with decreasing Cu loading amounts could be explained in three ways: (1) CuO species on the external surface of Cu-SSZ-13 catalyst have weak interaction with the zeolite acid sites, which leads to lower NH_3-SCR reaction rates; (2) some Cu^{2+} ions are much more active than the other ions; or (3) the SCR reaction is controlled by intraparticle diffusion limitations (interparticle diffusion limitations can be safely ruled out from Figure 12). For Fe-Cu-SSZ-13 catalysts, TOF drops off as the iron content increases, indicating that TOF varied with iron loading amounts, which is possible due to the existence of different fractions of iron species as iron exchange degree varies. It indicates that the NO reduction ability of the iron species is different in different Fe-Cu-SSZ-13 catalysts for NH_3-SCR reaction.

The results of characterization and activity test suggest that the activities of Fe-Cu-SSZ-13 catalysts should be related to the types, the quantities and locations of Cu and Fe species. The following discussion sections will supply more information about the structure-activity relationship of Fe-Cu-SSZ-13 catalysts in the NH_3-SCR reaction.

Discussion

Locations of Cu and Fe species in SSZ-13 molecular sieve

The CHA topology consists of a three-dimensional porous system with cavities and small-pore, eight-member ring windows with a free diameter (3.8 × 3.8 Å). However, the presence of small-pore windows in combination with the hydrophilic nature of aluminosilicates makes the introduction of catalytically active metal sites more difficult in SSZ-13,

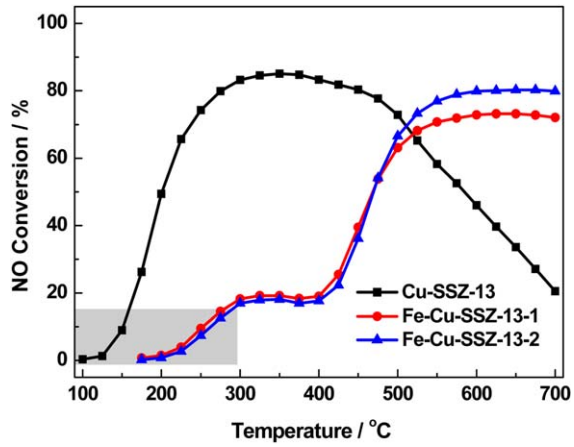

Figure 13. NO conversion versus reaction temperature for standard NH_3-SCR over Cu-SSZ-13 and Fe-Cu-SSZ-13 samples.

The differential regime (NO conversion $\leq$ 15%) is marked gray. Reaction mixture contains 1000 ppm NO, 1000 ppm NH_3, 3% O_2. GHSV = 800,000 h^{-1}. [Color figure can be viewed in the online issue, which is available at wileyonlinelibrary.com.]

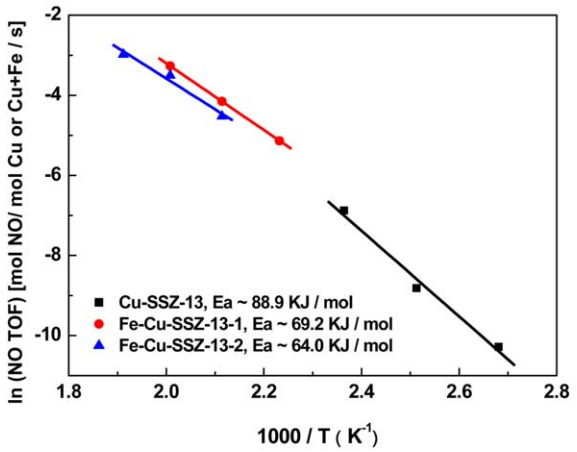

Figure 14. Arrhenius plots of NO conversion (in TOF, mol NO/mol Cu or Fe + Cu/s) over Cu-SSZ-13 and Fe-Cu-SSZ-13 catalysts.

TOFs were calculated using reaction data shown in Figure 13 within the differential regime. Reaction mixture contains 1000 ppm NO, 1000 ppm NH_3, 3% O_2 balanced with N_2, at a GHSV = 800,000 h^{-1}. [Color figure can be viewed in the online issue, which is available at wileyonlinelibrary.com.]

especially by aqueous exchange. Vennestrøm et al. found that the introduction of Cu into SAPO-34 occurred only in the outer parts of the crystals during aqueous ion exchange, which rendered a catalytically inactive material.[46] But upon the direct preparation of Cu-SSZ-13 zeolite, copper species are introduced in the CHA cages, giving a relatively homogeneous distribution.

According to the results of XRD and HRTEM, some CuO nanoparticles were anchored on the surface of Cu-SSZ-13 catalyst, and partial CuO particles gathered together with different sizes. This phenomenon indicates that the Cu loading amounts were very high in the initial product, and the part of Cu species would migrate and transform during the thermal treatment process. The results of H_2-TPR show that CuO nanoparticles account for a small part of Cu species in Cu-SSZ-13 catalyst (Supporting Information Figure S3). For Fe-Cu-SSZ-13 samples, no visible oxide species were discernible on their surface.

To confirm the position of most of Cu and Fe species in the catalysts, Cu-SSZ-13 and Fe-Cu-SSZ-13-1 samples were measured by FTIR spectra of adsorbed pyridine. It has been previously described in the literature that Cu-exchanged ZSM-5 zeolite exposed to pyridine shows a relatively intense band at 1450 cm^{-1}, assigned to pyridine adsorbed on Cu ions.[47] As shown in Figure 15d, the Cu-exchanged ZSM-5 zeolite demonstrates different bands associated with physically adsorbed pyridine species, such as the aforementioned band. Notably, ZSM-5 zeolite presents relatively large-pore channels and pyridine molecules can diffuse into them. However, SSZ-13 zeolite demonstrates exclusively small pores in its structure and, consequently, pyridine molecules could not diffuse through SSZ-13 channels. Therefore, pyridine would only interact with Cu ions on the external surface of the zeolite crystallites. The IR results of pyridine adsorbed on the Cu-SSZ-13 sample reveal that there are almost no signals (Figure 15a). It is a clear indication that most of Cu ions are located inside the cages of Cu-SSZ-13 samples, which are not accessible to pyridine. The Py-IR results of Fe-Cu-SSZ-13-1 also indicate Cu and Fe species are located inside its cages (Figure 15b).

XPS using an Mg Kα x-ray source gives an average sampling depth of ~4.5 nm for Cu 2p and Fe 2p and for microporous materials such as the CHA structure, which is slightly increased as a result of the large void fraction in zeolite materials.[48] Thus, more than 2–3 hexagonal unit cells with 36 T-atoms are probed in this way. Based on the ICP results of Fe-Cu-SSZ-13 samples (Table 1), it could be found that the content of Cu species is higher than that of Fe species. However, the XPS results of Fe-Cu-SSZ-13 samples show that the Cu 2p peak could not be observed, whereas the Fe 2p peak is obvious. This suggests that the copper and iron species are not homogeneously distributed. The former is in the internal parts of the crystals, and the latter is in the outer parts of the crystals. There are two possible reasons for these results. First, the introduction of Cu into SSZ-13 occurs in the synthesis process of carrier, this renders Cu^{2+} into ion-exchange sites more facile, and then increasing homogeneous distribution of active copper sites in the crystals. After consecutive ion exchange, Cu species in the outer parts of the crystals were exchanged and left some only in the internal parts of the crystals. Second, the presence of small-pore windows in combination with the hydrophilic nature of aluminosilicates makes the introduction of catalytically active iron sites more difficult in Cu-SSZ-13, especially by aqueous exchange. Herein, it reveals that during aqueous ion exchange, the introduction of Fe to Cu-SSZ-13 occurs only in the outer parts of the crystals. An extension in the ion-exchange time did not yield a corresponding distinct increase in iron content.

Relation between nature of copper and iron species and their catalytic activities

To understand structure-activity relationships of Fe-Cu-SSZ-13 catalysts for SCR reactions, the comparison and correlation of copper and iron species with SCR activity are made.

A number of stable Cu species in Cu-zeolites have been postulated to be active sites in the SCR reaction, such as dimeric Cu species, isolated cationic species, and even CuO_x nanoclusters.[49,50] On the base of UV-Vis study, Giordanino et al. excluded the presence of mono(μ-oxo)dicopper $[Cu\text{-}O\text{-}Cu]^{2+}$ dimmers within SSZ-13 framework by the absence of a

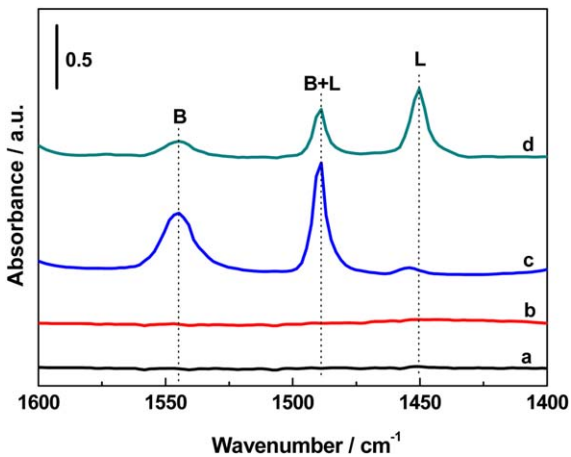

Figure 15. IR spectra after pyridine adsorption, followed by evacuation at 200°C, on Cu-SSZ-13 (a); Fe-Cu-SSZ-13-1 (b); HZSM-5 (c); Cu-ZSM-5 (d).

[Color figure can be viewed in the online issue, which is available at wileyonlinelibrary.com.]

band around 440 nm related to $[Cu\text{-}O\text{-}Cu]^{2+}$ dimmers.[51] Korhonen et al. confirmed the absence of Cu-dimers on their Cu-SSZ-13 sample (Si/Al = 9 and 2.9 wt % Cu).[52] Fickel and Lobo also found Cu^{2+} monomers in their dehydrated Cu-SSZ-13 catalyst at an ion-exchange level of 70% (4.39 wt % Cu, Si/Al = 6, and Cu/Al = 0.35) on the base of Rietveld refinement for TRXRD data.[4] In the present study, the results of UV-Vis (Figure 6) clearly rule out the presence of $[Cu\text{-}O\text{-}Cu]^{2+}$ dimers in Fe-Cu-SSZ-13 samples. The results of HRTEM and H_2-TPR have proved that a small part of Cu ions as copper oxide phase (e.g., CuO) only exist on the external surface of Cu-SSZ-13, and no visible copper oxide species were discernible on the external surface of Fe-Cu-SSZ-13 samples. Combined with the EPR results, the monomeric Cu^{2+} ions coordinated to three oxygen atoms on the six-ring sites are active copper species in Fe-Cu-SSZ-13. Furthermore, Lewis acid (copper ion) site-adsorbed ammonia species are more active, and selective to produce N_2 and water, than proton site-adsorbed ammonia species at low temperatures.[53] Therefore, Cu-SSZ-13 catalyst shows higher catalytic reactivity at low temperatures because of the more monomeric Cu^{2+} ions in it.

For iron species, any of the mononuclear iron ions, oligomeric Fe_xO_y clusters, or even iron oxide particles likely became active sites for SCR reaction in the different temperature ranges.[54,55] Høj et al. proposed that low iron loadings (1.2 wt % Fe) should result in mostly iron monomers, especially for the ion-exchanged samples.[56] Brandenberger et al. found that in zeolites with Fe/Al < 0.04 the formation of oxygen-bridged Fe-O-Fe species is not favored.[57] In the UV-Vis spectra (Figure 6) the majority of iron is present as iron monomers at the ion exchange positions, accompanied by a characteristic charge transfer band centered at about 206 and 280 nm. The results of EPR spectroscopy (Figure 8b) show that paramagnetic iron is present on Fe-Cu-SSZ-13 samples, as is expected for iron monomers. Thus, it might be concluded that the iron monomers contribute to the SCR activity of Fe-Cu-SSZ-13 catalysts at high temperatures.

Effect of Fe monomers on the catalytic behavior of Cu-SSZ-13 catalyst

It is well known that the transition metals, which are known to be good oxidation catalysts, are also good SCR catalysts. This is consistent with the fact that oxidation of NO to NO_2 is the rate-determining step in the SCR mechanism.[58] Kröcher and coworkers have measured the SCR, NO oxidation, and NH_3 oxidation activities of Cu-, Fe-, and Ag-ZSM-5 and found that the SCR activity is correlated with the oxidation activity of the redox metals at relatively low temperatures, that is, the higher the oxidation activity of the metal the higher the SCR activity.[58] At higher temperatures, however, the SCR activity follows the order: Ag-ZSM-5 > Fe-ZSM-5 > Cu-ZSM-5. The reason is that the reaction of ammonia with oxygen is more likely to happen on Cu-ZSM-5 catalyst, which has the strongest oxidation potential, and then the undesired oxidation of NH_3 starts to compete with the SCR reaction, leading to negligible formation of the undesirable products NO_x or N_2O.[59] In addition, Schwidder et al. found that NO and NH_3 conversions over Fe-ZSM-5 catalysts of low Fe content (Fe content less than or equal to 0.3 wt %) are equal in the whole temperature range. That is, the ammonia oxidation activity of these catalysts is very small.[60]

Thus, on the basis of the above literatures and obtained results, we are able to explain the effect of Fe monomers on the SCR activity over Cu-SSZ-13 catalyst. At low temperatures, Fe monomers show low activity, and the SCR reaction proceeds primarily over the more active Cu sites in the internal parts of the crystals. At higher temperatures, although the reaction of ammonia with oxygen is more likely to happen on Cu sites, the SCR activity of Fe monomers significantly increases. Then, the SCR reaction occurs increasingly over Fe monomers in the outer parts of the crystals, and thus the majority of the introduced ammonia is already converted before reaching Cu sites. Therefore, compared with Cu-SSZ-13, Fe-Cu-SSZ-13 catalysts have better catalytic performances at high temperatures. In combination with the results of activity test and ICP study, a small concentration of isolated Fe sites (0.089 wt %) is sufficient to sustain the high activity of Fe-Cu-SSZ-13-1 catalyst at high temperatures. Moreover, the iron species (Fe^{3+}/Fe^{2+}) formed and their redox properties might influence the catalytic activity of Fe-Cu-SSZ-13 catalysts.

Influence of intracrystalline diffusion limitations

Zeolite-based catalysts have some advantages of providing the site of ion exchange for highly dispersed and coordinately unsaturated cations, endowing acidic active sites, and enriching the reactants in zeolite pore, and so on. Contrary to these good points, zeolite channel structure might have negative effects on catalytic performance. The most plausible negative effect may be seen in a diffusion-limited reaction, in which the rate of mass transfer in zeolite channels cannot keep up with the intrinsic reaction rate.[61] It is because that the mass transfer in the intracrystalline space of zeolites is sometimes quite slow depending on the interactions between diffusing molecules and the walls of zeolite channels and on the closeness of the size of molecules to that of the channels, and, therefore, it is called configurational diffusion.[62] This effect should be more important for highly active catalysts, because it becomes larger as the ratio of intrinsic reaction rate to diffusion rate increases. Thus, the intracrystalline diffusivity must be an important factor for the design of highly active catalysts for the SCR of NO. Recently, Peden and coworkers have shown that intracrystalline (pore) diffusion limitations play significant roles in the low-temperature kinetics for Cu-SSZ-13 catalysts.[44] This situation is also found for our Cu-SSZ-13 and Fe-Cu-SSZ-13 catalysts. As shown in Figure 14 and Supporting Information Figure S6, reaction activation energies for Cu-SSZ-13 and Cu-SSZ-13-1 samples differ significantly even though the nature of the active Cu moieties is expected to be the same (i.e., isolated Cu^{2+} ions). Compared with Cu-SSZ-13-1 sample, the reaction activation energies of Fe-Cu-SSZ-13 samples increase dramatically even if the small amount of Fe is added. All of these experimental findings can be understood by considering the effect of diffusion limitations.

Under pore diffusion limitation, true apparent reaction activation energies (E_t) are modified by a diffusion activation energy (E_D) term such that the observed apparent activation energy is given by $E_{ob} = (E_t + E_D)/2$.[45] Because the average pore openings for the CHA materials are very small (3.8 Å), E_D may become much higher than 0. Compared with E_a of Peden's and Nam's ($\sim$62 kJ/mol),[44,63] Cu-SSZ-13 shows a relatively high E_a of 88.9 kJ/mol, suggesting fewer pore diffusion limitations. Cu-SSZ-13-1 sample shows the smallest E_a at 47.9 kJ/mol, indicating more severe such limitations. After Fe addition, Fe-Cu-SSZ-13-1 sample shows enhanced SCR activity with markedly increased E_a, indicating at least some reduction

of pore diffusion limitations. These phenomena may be due to the effect of the different locations of Cu and Fe species on the diffusion limitation. For Cu-SSZ-13 sample, more severe pore diffusion limitations would take place with ammonium exchange. During ammonium exchange, Cu^{2+} ions in the outer parts of the crystals were first exchanged, thereby aggravating pore diffusion limitations. After Fe ion exchange, the introduction of active Fe species into Cu-SSZ-13 occurs only in the outer parts of the crystals, which is in favor of reducing such limitations.

Conclusions

1. The operation temperature window of Cu-SSZ-13 catalyst was widened due to the addition of a small amount of iron. The selected Fe-Cu-SSZ-13-1 catalyst exhibited the high NO conversion (>90%) in the wide temperature range (225–625°C), which also showed good N_2 selectivity and excellent hydrothermal stability.
2. The locations of Cu and Fe species in SSZ-13 molecular sieve were confirmed. The results of Py-IR showed that the Cu and Fe species of Fe-Cu-SSZ-13 catalyst were mainly located inside the cages of the SSZ-13 crystals. The results of XPS suggested that Cu species were in the internal parts of the SSZ-13 crystals, and Fe species are in the outer parts of the SSZ-13 crystals.
3. The active species of Fe-Cu-SSZ-13 catalysts were determined. The results of UV-Vis and EPR showed that the monomeric Cu^{2+} ions coordinated to three oxygen atoms on the six-ring sites are active Cu species in Fe-Cu-SSZ-13 catalysts, and the Fe monomers contribute to the SCR activity of Fe-Cu-SSZ-13 catalysts at high temperatures.
4. The low-temperature NH_3-SCR kinetics was controlled by intracrystalline mass-transfer limitations for the Fe-Cu-SSZ-13 catalysts. The exchange of the active Cu species in the outer parts of the crystals may aggravate these limitations. However, the introduction of active Fe species to Cu-SSZ-13 occurring only in the outer parts of the crystals may, in contrast, significantly reduce such limitations.

Acknowledgment

This work was supported by the National Natural Science Foundation of China (Nos. 21173270, 21376261, and 21177160), the 863 program of China (2013AA065302), the Doctor select Foundation (20130007110007), and Beijing NSF (2142027).

Literature Cited

1. Topsøe NY. Mechanism of the selective catalytic reduction of nitric oxide by ammonia elucidated by in situ on-line Fourier transform infrared spectroscopy. *Science*. 1994;265:1217–1219.
2. Moliner M, Martínez C, Corma A. Synthesis strategies for preparing useful small pore zeolites and zeotypes for gas separations and catalysis. *Chem Mater*. 2014;26:246–258.
3. Kwak JH, Tonkyn RG, Kim DH, Szanyi J, Peden CHF. Excellent activity and selectivity of Cu-SSZ-13 in the selective catalytic reduction of NO*x* with NH_3. *J Catal*. 2010;275:187–190.
4. Fickel DW, Lobo RF. Coordination in Cu-SSZ-13 and Cu-SSZ-16: investigated by variable-temperature XRD. *J Phys Chem C*. 2010; 114:1633–1640.
5. Fickel DW, D'Addio E, Lauterbach JA, Lobo RF. The ammonia selective catalytic reduction activity of copper-exchanged small-pore zeolites. *Appl Catal B Environ*. 2011;102:441–448.
6. Bull I, Boorse RS, Jaglowski WM, Koermer GS, Moini A, Patchett JA, Xue WM, Burk P, Dettling JC, Caudle MT. Copper CHA zeolinte catalysts. U.S. Patent 0,226,545, 2008.
7. Kwak JH, Tran D, Burton SD, Szanyi J, Lee JH, Peden CHF. Effects of hydrothermal aging on NH_3-SCR reaction over Cu/zeolites. *J Catal*. 2012;287:203–209.
8. Ren L, Zhu L, Yang C, Chen Y, Sun Q, Zhang H, Li C, Nawaz F, Xiao F-S. Designed copper-amine complex as efficient template for one-pot synthesis of Cu-SSZ-13 zeolite with excellent activity for selective catalytic reduction of NO*x* by NH_3. *Chem Commun*. 2011; 47:9789–9791.
9. Ren L, Zhang Y, Zeng S, Zhu L, Sun Q, Zhang H, Yang C, Meng X, Yang X, Xiao F-S. Design and synthesis of a catalytically active Cu-SSZ-13 zeolite from a copper-amine complex template. *Chin J Catal*. 2012;33:92–105.
10. Xie L, Liu F, Ren L, Shi X, Xiao F-S, He H. Excellent performance of one-pot synthesized Cu-SSZ-13 catalyst for the selective catalytic reduction of NO*x* with NH_3. *Environ Sci Technol*. 2014;48:566–572.
11. Xie L, Liu F, Liu K, Shi X, He H. Inhibitory effect of NO_2 on the selective catalytic reduction of NO*x* with NH_3 over one-pot synthesized Cu-SSZ-13 catalyst. *Catal Sci Technol*. 2014;4:1104–1110.
12. Martínez-Franco R, Moliner M, Franch C, Kustov A, Corma A. Rational direct synthesis methodology of very active and hydrothermally stable Cu-SAPO-34 molecular sieves for the SCR of NO*x*. *Appl Catal B Environ*. 2012;127:273–280.
13. Martínez-Franco R, Moliner M, Thogersen JR, Corma A. Efficient one-pot preparation of Cu-SSZ-13 materials using cooperative OSDAs for their catalytic application in the SCR of NO*x*. *ChemCatChem*. 2013;5:3316–3323.
14. Martínez-Franco R, Moliner M, Concepcion P, Thogersen JR, Corma A. Synthesis, characterization and reactivity of high hydrothermally stable Cu-SAPO-34 materials prepared by "one-pot" processes. *J Catal*. 2014;314:73–82.
15. Kim YJ, Kwon HJ, Heo I, Nam I-S, Cho BK, Choung JW, Cha M-S, Yeo GK. Mn-Fe/ZSM5 as a low-temperature SCR catalyst to remove NO*x* from diesel engine exhaust. *Appl Catal B Environ*. 2012;126:9–21.
16. Sultana A, Sasaki M, Suzuki K, Hamada H. Tuning the NO_x conversion of Cu-Fe/ZSM-5 catalyst in NH_3-SCR. *Catal Commun*. 2013; 41:21–25.
17. Yang X, Wu Z, Moses-Debusk M, Mullins DR, Mahurin SM, Geiger RA, Kidder M, Narula CK. Heterometal incorporation in metal-exchanged zeolites enables low-temperature catalytic activity of NO*x* reduction. *J Phys Chem C*. 2012;116:23322–23331.
18. Zhang R, Li Y, Zhen T. Ammonia selective catalytic reduction of NO over Fe/Cu-SSZ-13. *RSC Adv*. 2014;4:52130–52139.
19. Zhang T, Liu J, Wang D, Zhao Z, Wei Y, Cheng K, Jiang G, Duan A. Selective catalytic reduction of NO with NH_3 over HZSM-5-supported Fe-Cu nanocomposite catalysts: the Fe-Cu bimetallic effect. *Appl Catal B Environ*. 2014;148–149:520–531.
20. Treacy MMJ, Higgins JB. *Collection of Simulated XRD Patterns for Zeolites*, 5th ed. Amsterdam: Elsevier, 2007:112–115.
21. Qi G, Yang RT. Selective catalytic oxidation (SCO) of ammonia to nitrogen over Fe/ZSM-5 catalysts. *Appl Catal A Gen*. 2005;287:25–33.
22. Wang W, Zhou Q, Fei X, He Y, Zhang P, Zhang G, Peng L, Xie W. Synthesis of CuO nano- and micro-structures and their Raman spectroscopic studies. *CrystEngComm*. 2010;12:2232–2237.
23. Martins GAV, Berlier G, Coluccia S, Pastore HO, Superti GB, Gatti G, Marchese L. Revisiting the nature of the acidity in chabazite-related silicoaluminophosphates: combined FTIR and ^{29}Si MAS NMR study. *J Phys Chem C*. 2007;111:330–339.
24. Ismagilov ZR, Yashnik SA, Anufrienko VF, Larina TV, Vasenin NT, Bulgakov NN, Vosel SV, Tsykoza LT. Linear nanoscale clusters of CuO in Cu-ZSM-5 catalysts. *Appl Surf Sci*. 2004;226:88–93.
25. Kumar MS, Schwidder M, Grünert W, Brückner A. On the nature of different iron sites and their catalytic role in Fe-ZSM-5 DeNO*x* catalysts: new insights by a combined EPR and UV/VIS spectroscopic approach. *J Catal*. 2004;227:384–397.
26. Kim MH, Nam I-S, Kim YG. Characteristics of mordenite-type zeolite catalysts deactivated by SO_2 for the reduction of NO with hydrocarbons. *J Catal*. 1998;179:350–360.
27. Chaswick D, Hashemi T. Adsorbed corrosion inhibitors studied by electron spectroscopy: benzotriazole on copper and copper alloys. *Corros Sci*. 1978;18:39–51.
28. Gong J, Yue H, Zhao Y, Zhao S, Zhao L, Lv J, Wang S, Ma X. Synthesis of ethanol via syngas on Cu/SiO_2 catalysts with balanced Cu^0-Cu^+ Sites. *J Am Chem Soc*. 2012;134:13922–13925.

29. Nedyalkova R, Kamasamudram K, Currier NW, Li J, Yezerets A, Olsson L. Experimental evidence of the mechanism behind NH_3 over consumption during SCR over Fe-zeolites. *J Catal*. 2013;299: 101–108.
30. Nedyalkova R, Shwan S, Skoglundh M, Olsson L. Improved low-temperature SCR activity for Fe-BEA catalysts by H_2-pretreatment. *Appl Catal B Environ*. 2013;138–139:373–380.
31. Rivallan M, Ricchiardi G, Bordiga S, Zecchina A. Adsorption and reactivity of nitrogen oxides (NO_2, NO, N_2O) on Fe-zeolites. *J Catal*. 2009;264:104–116.
32. Xue J, Wang X, Qi G, Wang J, Shen M, Li W. Characterization of copper species over Cu/SAPO-34 in selective catalytic reduction of NO*x* with ammonia: relationships between active Cu sites and de-NO*x* performance at low temperature. *J Catal*. 2013;297:56–64.
33. Ma L, Cheng Y, Cavataio G, McCabe RW, Fu L, Li J. Characterization of commercial Cu-SSZ-13 and Cu-SAPO-34 catalysts with hydrothermal treatment for NH_3-SCR of NO*x* in diesel exhaust. *Chem Eng J*. 2013;225:323–330.
34. Tuel A, Acron I, Millet JMM. Investigation of structural iron species in Fe-mesoporous silicas by spectroscopic techniques. *J Chem Soc Faraday Trans*. 1998;94:3501–3510.
35. Schwidder M, Kumar MS, Brückner A, Grünert W. Active sites for NO reduction over Fe-ZSM-5 catalysts. *Chem Commun*. 2005;6: 805–807.
36. Sultana A, Nanba T, Sasaki M, Haneda M, Suzuki K, Hamada H. Selective catalytic reduction of NO*x* with NH_3 over different copper exchanged zeolites in the presence of decane. *Catal Today*. 2011; 164:495–499.
37. Matins GVA, Berlier G, Bisio C, Coluccia S, Pastore HO, Marchese L. Quantification of brønsted acid sites in microporous catalysts by a combined FTIR and NH_3-TPD study. *J Phys Chem C*. 2008;112: 7193–7200.
38. Onida B, Gabelica Z, Lourencüo J, Garrone E. Spectroscopic characterization of hydroxyl groups in SAPO-40. 1. Study of the template-free samples and their interaction with ammonia. *J Phys Chem*. 1996;100:11072.
39. Choudhary VR, Akolekar DB. Comparison of the acidity/site energy distribution in catalytically important zeolites. *J Catal*. 1989;119: 525–530.
40. Kuehl GH, Timken HKC. Acid sites in zeolite beta: effects of ammonium exchange and steaming. *Microporous Mesoporous Mater*. 2000;35–36:521–532.
41. Dwyer J. A critical evaluation of the concept of Brønsted acidity related to zeolites. In: Grobet PJ, Mortier WJ, Vansant EF, editors. *Innovation in Zeolite Materials Science*. Amsterdam: Elsevier, 1988: 333–354.
42. Sjövall H, Olsson L, Fridell E, Blint RJ. Selective catalytic reduction of NO*x* with NH_3 over Cu-ZSM-5: the effect of changing the gas composition. *Appl Catal B Environ*. 2006;64:180–188.
43. Li J, Chang H, Ma L, Hao J, Yang RT. Low-temperature selective catalytic reduction of NO*x* with NH_3 over metal oxide and zeolite catalysts-a review. *Catal Today*. 2011;175:147–156.
44. Gao F, Walter ED, Karp EM, Luo J, Tonkyn RG, Kwak JH, Szanyi J, Peden CHF. Structure-activity relationships in NH_3-SCR over Cu-SSZ-13 as probed by reaction kinetics and EPR studies. *J Catal*. 2013;300:20–29.
45. Gao F, Walter ED, Washton NM, Szanyi J, Peden CHF. Synthesis and evaluation of Cu-SAPO-34 catalysts for ammonia selective catalytic reduction. 1. Aqueous solution ion exchange. *ACS Catal*. 2013; 3:2083–2093.
46. Vennestrøm PNR, Katerinopoulou A, Tiruvalam RR, Kustov A, Moses PG, Concepcion P, Corma A. Migration of Cu ions in SAPO-34 and its impact on selective catalytic reduction of NO*x* with NH_3. *ACS Catal*. 2013;3:2158–2161.
47. Sultana A, Nanba T, Haneda M, Sasaki M, Hamada H. Influence of co-cations on the formation of Cu^+ species in Cu/ZSM-5 and its effect on selective catalytic reduction of NO*x* with NH_3. *Appl Catal B Environ*. 2010;10:61–67.
48. Ross JRH. Heterogeneous Catalysis: Fundamentals and Applications. Amsterdam: Elsevier, 2012.
49. Guo Q, Fan F, Ligthart DAJM, Li G, Feng Z, Hensen EJM, Li C. Effect of the nature and location of copper species on the catalytic nitric oxide selective catalytic reduction performance of the copper/SSZ-13 zeolite. *ChemCatChem*. 2014;6:634–639.
50. Beutel T, Sárkány J, Lei G-D, Yan JY, Sachtler WMH. Redox chemistry of Cu/ZSM-5. *J Phys Chem*. 1996;100:845–851.
51. Giordanino F, Vennestrøm PNR, Lundegaard LF, Stappen FN, Mossin S, Beato P, Bordigaa S, Lamberti C. Characterization of Cu-exchanged SSZ-13: a comparative FT-IR, UV-Vis, and EPR study with Cu-ZSM-5 and Cu-β with similar Si/Al and Cu/Al ratios. *Dalton Trans*. 2013;42:12741–12761.
52. Korhonen ST, Fickel DW, Lobo RF, Weckhuysen BM, Beale AM. Isolated Cu^{2+} ions: active sites for selective catalytic reduction of NO. *Chem Commun*. 2011;47:800–802.
53. Zhu H, Kwak JH, Peden CHF, Szanyi J. In situ DRIFTS-MS studies on the oxidation of adsorbed NH_3 by NO*x* over a Cu-SSZ-13 zeolite. *Catal Today*. 2013;205:16–23.
54. Iwasaki M, Yamazaki K, Banno K, Shinjoh H. Characterization of Fe/ZSM-5 DeNO*x* catalysts prepared by different methods: relationships between active Fe sites and NH_3-SCR performance. *J Catal*. 2008;260:205–216.
55. Schwidder M, Grünert W, Bentrup U, Brückner A. Selective reduction of NO with Fe-ZSM-5 catalysts of low Fe content: part II. Assessing the function of different Fe sites by spectroscopic in situ studies. *J Catal*. 2006;239:173–186.
56. Høj M, Beier MJ, Grunwaldt JD, Dahl S. The role of monomeric iron during the selective catalytic reduction of NO*x* by NH_3 over Fe-BEA zeolite catalysts. *Appl Catal B Environ*. 2009;93:166–176.
57. Brandenberger S, Kröcher O, Tissler A, Althoff R. Estimation of the fractions of different nuclear iron species in uniformly metal-exchanged Fe-ZSM-5 samples based on a Poisson distribution. *Appl Catal A Gen*. 2010;373:168–175.
58. Brandenberger S, Kröcher O, Tissler A, Althof R. The state of the art in selective catalytic reduction of NO*x* by ammonia using metal-exchanged zeolite catalysts. *Catal Rev*. 2008;50:492–531.
59. Kröcher O, Elsener M. Combination of V_2O_5/WO_3-TiO_2, Fe-ZSM5, and Cu-ZSM5 catalysts for the selective catalytic reduction of nitric oxide with ammonia. *Ind Eng Chem Res*. 2008;47:8588–8593.
60. Schwidder M, Kumar MS, Klementiev K, Pohl MM, Brückner A, Grünert W. Selective reduction of NO with Fe-ZSM-5 catalysts of low Fe content: I. Relations between active site structure and catalytic performance. *J Catal*. 2005;231:314–330.
61. Post MFM. Chapter 11 diffusion in zeolite molecular sieves. *Stud Surf Sci Catal*. 1991;58:391–444.
62. Snurr RQ, Hagen A, Ernst H, Schwarz HB, Ernst S, Weitkamp J, Karger J. *In situ* PFG NMR study of intracrystalline diffusion during ethene conversion in ZSM-5. *J Catal*. 1996;163:130–137.
63. Kim YJ, Lee JK, Min KM, Hong SB, Nam I-S, Cho BK. Identification of nitrites/HONO as primary products of NO oxidation over Fe-ZSM-5 and their role in the standard SCR mechanism: a chemical trapping study. *J Catal*. 2014;311:447–457.

Manuscript received Feb. 7, 2015, and revision received May 30, 2015.